Chapter 6

Physical Reasons of Emission Varying in CdSe/ZnS and CdSeTe/ZnS Quantum Dots at Bioconjugation to Antibodies

Tetyana V. Torchynska

Additional information is available at the end of the chapter

http://dx.doi.org/10.5772/60821

Abstract

Photoluminescence, its excitation power dependence, and Raman scattering spectra have been studied in CdSe/ZnS and CdSeTe/ZnS QDs for the nonconjugated states and after the QD conjugation to the anti-Interleukin-10, Human papilloma virus and Pseudo rabies virus antibodies. The QD bioconjugation to charged antibodies stimulates the "blue" energy shift of PL bands related to exciton emission in the CdSe or CdSeTe cores. The "blue" energy shift of PL spectrum in bioconjugated CdSe/ZnS QDs has been attributed to the electronic quantum confined effects stimulated by decreasing the effective QD size at its bioconjugation to charged antibodies. It was shown that the attachment of a charge deals with the antibody to the exterior shell of CdSe/ZnS QDs, leads to blocking away a fraction of core's volume. The energy band diagrams of CdSeTe/ZnS QDs in the nonconjugated and bioconjugated states have been designed, which permit to explain the types of optical transitions in QDs and their transformations at the QD bioconjugation. It is shown that the change of energy band profile and the "blue" shift of QD energy levels, owing to the change of potential barrier at the QD surface, are the dominant reasons of PL spectrum transformation in the double core CdSeTe/ZnS QDs conjugated to charged antibodies. Better understanding the QD bioconjugation to specific antibodies is expected to produce the major advances in biology and medicine and can be a powerful technique for early medical diagnostics.

Keywords: CdTeSe/ZnS quantum dots, CdSe/ZnS quantum dots, emission, bioconjugation

1. Introduction

In the last two decades, the colloidal core/shell quantum dots (QDs) of II-VI semiconductors (CdSe, CdS, CdSeTe, and ZnS) attracted an enormous scientific attention owing to the fundamental scientific aspects and future promising applications in optoelectronics, photonics, biology, and medicine. The modern developments in nanotechnology allow numerous promising applications in the field of biology and medicine, which in the future may bring an unprecedented effect in nanomedicine [1, 2].

The development of biocompatible nanoparticles for molecular imaging and targeted therapy is an area of enormous current interest. This novel technique as expected will allow targeted drug delivery to cells with certain parameters, as well as improvements in diagnostics and localization of affected tissues in the human body. When conjugated with biomolecular affinity ligands, such as antibodies, peptides, or small molecules, these nanoparticles can be used to target malignant specific tumors [3-5].

The key issue for nanoparticles intended for biological use is to ensure their stability, which suggests the formation of core-shell structures with a certain enveloping layer required to isolate a nanoparticle [6]. The core defines the main properties of the system—it may be the material with outstanding luminescence or magnetic properties for the precise detection of particle's location inside the body. On the other hand, the core can be used as a reservoir for the medicine used in targeted drug delivery applications. The application of semiconductor QDs as luminescent markers in biology and medicine is expected to produce the major advances in molecular diagnostic [1], gene technology [2], toxin detections [7], drag delivery [8], at obtaining tissue imaging in vivo etc [3, 9].

Note that luminescent markers usually used earlier, such as organic dyes, fluorescent proteins, or lanthanide chelates, have some restrictions, such as broad spectrum bands, low photo bleaching threshold, poor photochemical stability, and degradation [10]. In contrary, the II-VI semiconductor core/shell QDs are characterized by the high-photoluminescence (PL) quantum yield (up to 75%) [11-13]. Surface-passivized II-VI QDs are highly stable against photo bleaching and are characterized by narrow, symmetric emission peaks with the half width about 25-30 nm [6].

New luminescent markers are needed for the better assessment of treatments for many types of cancers. The antibodies, which can be found in circulating blood, may help in the early detection of cancer. The development of a blood test, using the optical methods, which permits early diagnosis, would be a great advance in the management of cancer disease. Note that the core/shell CdSeTe/ZnS QDs with near-infrared (IR) emission (780-800 nm) are very interesting for biological applications owing to the possibility of animal imaging in vivo due to the low absorption of IR light by an animal tissue [6, 14, 15]. At the same time, the chemical behavior of Cd/Se/Te components of QDs in the biological system is still unclear. The last question is very important due to the toxicity of these components for the human body [16-18].

The conjugation of biomolecules with semiconductor core/shell QDs has been achieved using functional groups (linkers) on the QD surface [19-21], and/or with the help of electrostatic

http://dx.doi.org/10.5772/60821

interaction between the QDs and the biomolecules [12, 22, 23]. A set of publications, related to the study of QD bioconjugation using PL spectroscopy, revealed that the emission intensity of QDs decreased [12, 24, 25] or increased [22, 26] owing to the energy exchange between the QDs and the biomolecules. Thus, the QD luminescence intensity depends on the concentration of attached biomolecules, promising the QD application as a protein sensor as well [6]. However, the limits of biomolecule detection are not very sensitive. Moreover, the influence of bioconjugation processes on QD optical properties and the bioconjugation mechanisms are not yet completely understood.

It is desirable to have the additional information concerning the conjugation process such as a spectral shift of QD emission or changing the PL band half width, or using nonlinear optical phenomena: two-photon-induced fluorescence, second harmonic generation, or sum frequency generation [27]. Simultaneously, the other optical methods can be useful for the bioconjugation detection such as the Raman scattering method [28] or coherent anti-Stokes Raman scattering (CARS) [27]. This chapter presents the study of the transformation of PL and Raman scattering spectra of the core/shell CdSe/ZnS QDs with visible emission (605 or 655 nm) and CdSeTe/ZnS QDs with near IR emission (780-800 nm) at the bioconjugation to different types of antibodies.

2. QD bioconjugation process and experimental details

Core-shell quantum dots (QDs) commercially available covered by the amine (NH_2)-derivatized polyethylene glycol (PEG) polymer were used in a form of colloidal particles diluted in a phosphate-buffered saline (PBS) with a 1:200 volumetric ratio. CdSe/ZnS QDs with emission peaked at 605 nm (2.05 eV) and 655 nm (1.89 eV) and CdSeTe/ZnS QDs with emission at 780-800 nm (1.55-1.60 eV) have been investigated. QDs have been studied by means of photoluminescence and Raman scattering methods in nonconjugated states and after the conjugation to different types of antibodies (Ab). All optical measurements are performed on the dried droplets of the original solution of nonconjugated and bioconjugated QDs. At the first the PL spectra of QDs are studied in the nonconjugated state. Then some part of QDs has been conjugated to the antibodies using the QD conjugation kits [29, 30]. These kits contain amine-derivatized polymer-coated QDs and the amine-thiol cross-linker SMCC. The samples of QDs (bioconjugated and nonconjugated) in the form of a 5-mm spot were dried on a surface of crystalline Si substrates (Figure 1) as described earlier by Torchynska [22] and Vega Macotela et al. [24].

The types of antibodies (Ab) used for the bioconjugation to the CdSe/ZnS QDs with emission at 605 nm (2.05 eV) and 655 nm (1.89 eV) are as follows:

i. Mouse monoclonal [8C9] antihuman papilloma virus Ab, HPV 16-E7, bacterially derived fusion protein containing anti-HPV 16 early protein E7 Ab (Invitrogen, isotype (IgG1))

ii. Anti-interleukin-10 (IL-10) antibodies (antihuman IL-10, Rt IgG1, stock concentration of 1 mg/ml, clone JES3-9D7, code RHCIL1000)

iii. Pseudorabies virus (PRV) Ab, immunoglobulin G antibodies (affinity purified with Protein G Sepharose from rabbit antiserum to pseudorabies virus, stock concentration of 1 mg/ml in PBS)

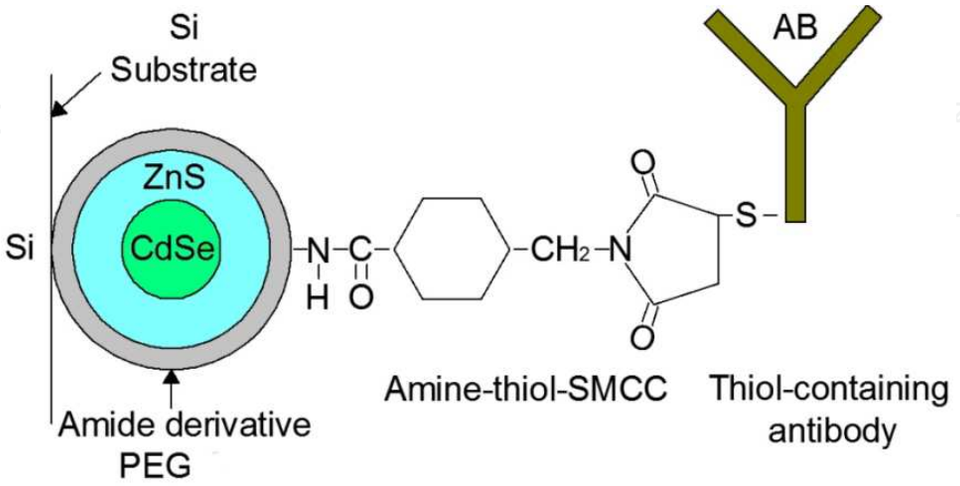

Figure 1. Bioconjugated CdSe/ZnS QDs on the Si substrate.

CdSeTe/ZnS QDs with near IR emission at 780-800 nm (1.59-1.60 eV) have been conjugated to different types of antibodies as well:

i. Mouse monoclonal [8C9] antihuman papilloma virus Ab, anti-HPV 16-E7, bacterially derived fusion protein containing anti-HPV 16 early protein E7 Ab (Invitrogen, isotype (IgG1))

ii. Mouse monoclonal [C1P5] antihuman papilloma virus HPV16 E6 + HPV18 E6 Ab, HPVE6 (Abcam, ab70, isotypeIgG1, gel-purified HPV18 E6-betagalacto-sidase fusion protein)

iii. Pseudorabies virus (PRV) Ab, immunoglobulin G antibodies (affinity purified with Protein G Sepharose from rabbit antiserum to Pseudorabies virus, stock concentration of 1 mg/ml in PBS)

iv. Anti-IL-10 antibodies (antihuman IL-10, Rt IgG1, stock concentration of 1 mg/ml, clone JES3-9D7, code RHCIL1000)

The protocol of bioconjugation details can be found in refs. [29, 30]. Bioconjugated CdSe/ZnS QDs have been called as 605P+IL-10, 655P+IL-10, 605P +HPV E7, 655P +HPV E7, 605P+PRV, and 655P+PRV, and the bioconjugated CdSeTe/ZnS QDs have been called as (i) 800P+HPV E7, (ii) 800P+HPV E6, (iii) 800P+PRV, and (iv) 800P+IL-10.

The majority of PL spectra were measured at the excitation by a He-Cd laser with a wavelength of 325 nm and a beam power of 76 mW at 300 K using a PL setup on a base of spectrometer SPEX500 described by Torchynska [22] and Vega Macotela et al. [24]. Raman scattering spectra were measured at 300 K by means of the spectrometer Lab-Raman HR800 Horiba Jovin-Yvon

http://dx.doi.org/10.5772/60821

in the range of Raman shifts of 100-600 cm^{-1} at the excitation by a solid-state laser with a wavelength of 532 nm and a beam power of 20 mW [26, 28].

3. The bioconjugation study of CdSe/ZnS QDs

3.1. CdSe/ZnS QDs bioconjugated to anti-IL-10 Ab

Figures 2 and 3 demonstrate the PL spectra of the three samples of nonconjugated (605N, 655N) QDs and three samples of bioconjugated (605P, 655P) QDs.

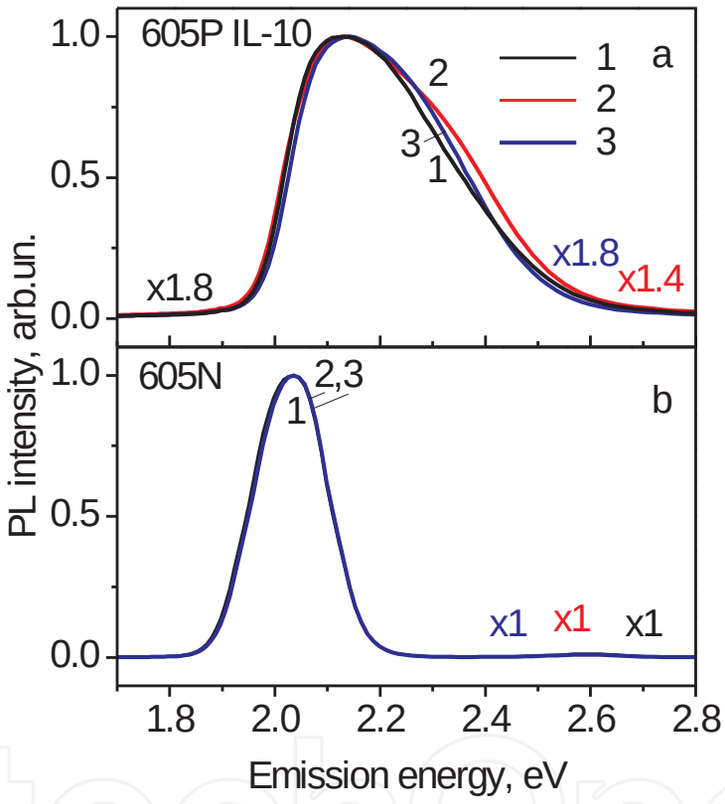

Figure 2. Normalized PL spectra of three 605P (a) and three 605N (b) QD samples at 300 K. Numbers at the curves (×1, ×1.4, and ×1.8) show the multiplication coefficients used at the normalization of PL spectra.

The PL spectra of CdSe/ZnS QDs are characterized by the Gaussian shape PL band in the nonconjugated states with the peaks at 2.04 eV (Figure 2) and 1.90 eV (Figure 3) related to exciton emission in corresponding CdSe cores [31]. At the bioconjugation of studied QDs, the PL intensity decreases, the emission peak shifts to higher energies, a PL half width increases, and the shape of PL bands became asymmetric with high-energy tails (Figures 2 and 3). The PL energy shift at the bioconjugation of QDs to antibodies can be attributed to the following: (i) the impact of anti-IL-10 Ab or PBS buffer emission excited by UV light, (ii) the oxidation or degradation of CdSe cores owing to core/shell atom intermixing [32], (iii) the impact of compressive strains that appears at the bioconjugation [33, 34], or (iv) the emission of excitons

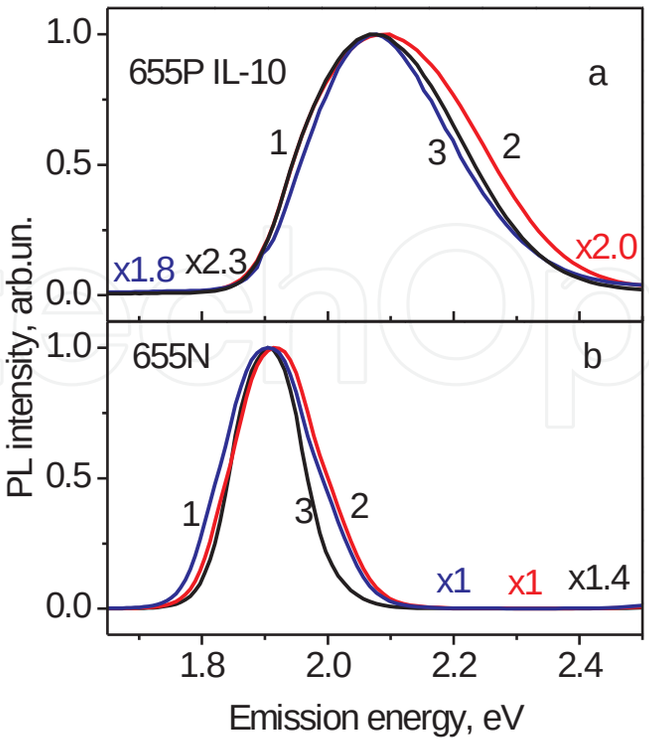

Figure 3. Normalized PL spectra of three655P (a) and three 655N (b) QD samples at 300 K. Numbers at the curves (×1, ×1.8, and ×2.0) show the multiplication coefficients used at the normalization of PL spectra.

bound to the QD excited states in QDs [31]. To distinguish between proposed reasons, the PL spectra of anti-IL-10 Ab and PBS were studied at UV light excitation (Figure 4).

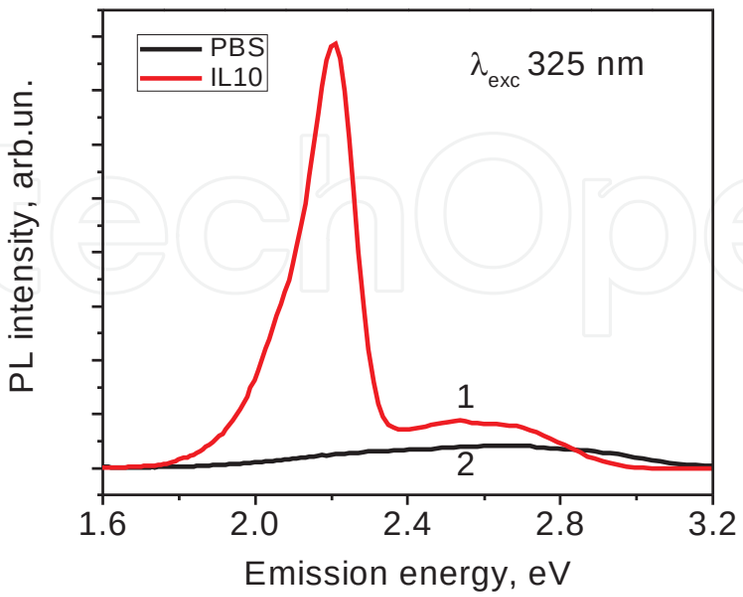

Figure 4. PL spectra of anti-IL-10 Ab (1) and PBS (2) without QDs.

http://dx.doi.org/10.5772/60821

The PL spectrum of anti-IL-10 Ab is characterized by the PL band with a maximum at 2.21 eV and a small shoulder in the range 2.4-3.0 eV (Figure 4, curve 1). The PL spectrum of PBS is shown in Figure 4, curve 2. The PL intensity of PBS in the range 2.2-3.2 eV is 15-fold smaller than the emission intensity of 2.21 eV PL band related to anti-IL-10 Ab. Simultaneously, the PL intensity of anti-IL-10 Ab emission (2.21 eV) is 10-fold smaller than the PL band intensity of CdSe/ZnS QDs at UV excitation. Hence, we can conclude that the "blue" shifts of PL spectra in bioconjugated QDs (605P and 655P) do not connect with the luminescence of anti-Il-10 Ab or PBS. However, the emission of anti-IL-10 Ab cans influent on the shape of tails in PL spectra of bioconjugated QDs.

Raman scattering spectra were investigated with the goal to study the impact of compressive strains [33, 34] and the oxidation or degradation processes at the QD bioconjugation [32, 35], as well as to confirm the existence of electric charges in IL-10 Ab. Raman scattering spectra of 605N and 605P CdSe/ZnS QDs present the low-intensity Raman peaks at 211.9, 235.8, 302.8, 345.3, 424.8, 434.6, and 490 cm^{-1} (Figure 5).

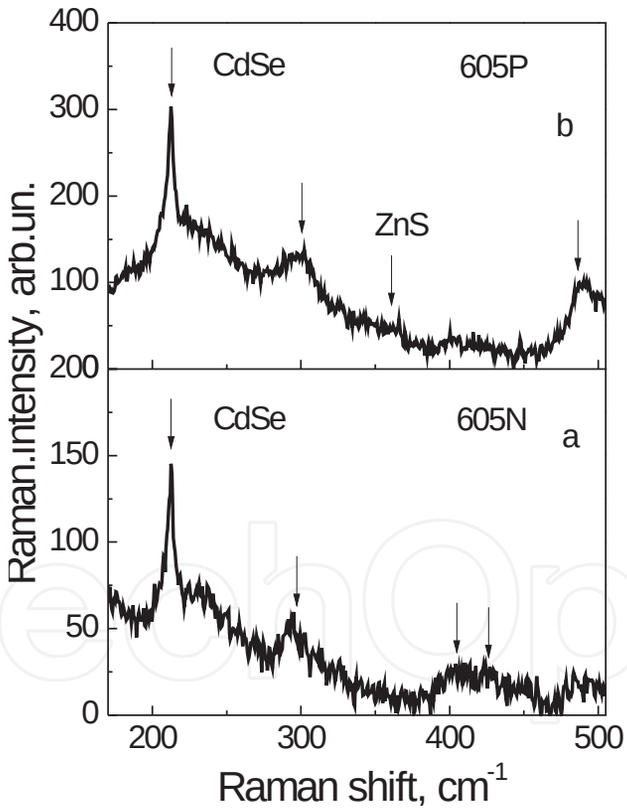

Figure 5. Raman scattering spectra of nonconjugated (a) and bioconjugated (b) QDs.

The peak at 211.9 cm^{-1} (and two phonon overtone at 424.8 cm^{-1}) corresponds to LO phonons in the CdSe core. The shift of LO phonon Raman peak (211.9 cm^{-1}) from its position in the bulk CdSe crystal (213 cm^{-1}) has related to the phonon confinement effect in small QDs [6, 35]. The peak at 345.3 cm^{-1} is due to the LO phonon scattering in the ZnS shell (Figure 5). The shift of

LO phonon Raman peak (345.3 cm^{-1}) from its position in the bulk ZnS crystal (352 cm^{-1}) is related to the phonon confinement effect in thin ZnS shell [6, 35, 36]. Raman spectra in the diapason of 0-500 cm^{-1} include the peaks related to the Si substrate as well (Figure 1). Raman scattering spectra of Si present the overtones of acoustic phonons: 235.8, 302.8, 434.6, and 458.6 cm^{-1} (Figure 5). The peaks at 230, 302, 435, and 469 cm^{-1} were attributed early to two TA phonon overtones at the L, X, and Σ critical points of the Si Brillouin zone [36-38].

The Raman study shows that Raman peaks related to LO phonons in the CdSe core (Figure 5) have not varied at the QD bioconjugation. Meanwhile, if the QD bioconjugation is accompanied by the compressive strain applied, and by the degradation or oxidation of cores, the Raman peaks have to change. Finally, we can conclude that the mentioned processes have not been realized at the QD bioconjugation to anti-IL-10 Ab.

Note that the CdSe core Raman peak intensity increases twofold in bioconjugated QDs as it is shown in Figure 5. The enhancement of optical field at the surface of bioconjugated QDs and increasing the Raman peak intensity can be attributed to the surface-enhanced Raman scattering (SERS) [28,39]. This fact means that anti-IL-10 Abs have the electric charges (dipoles), which interact with an electric field of excitation light at the SERS effect [39-41].

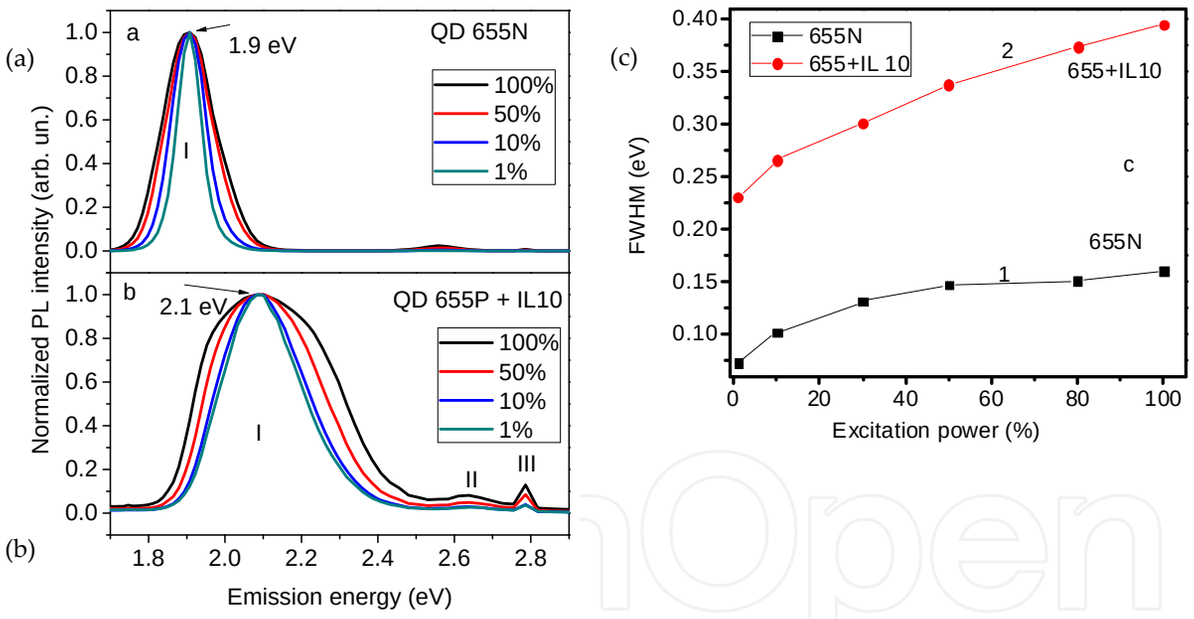

Figure 6. (a,b). Normalized PL spectra of 655N (a) and 655P-IL-10 (b) QDs at different excitation light intensities 100%, 50%, 10%, and 1%, respectively. The 100% intensity corresponds to 76 mW. Coefficients at the normalization of PL spectra for 655N QDs (a) are ×1.00, ×1.10, ×1.75, and ×9.11 and for 655P QDs (b) are ×1.28, ×1.59, ×3.38, and ×31.18. (c). FWHMs of main PL bands in PL spectra of 655N (1) and 655P-IL-10 (2) QDs versus excitation light power.

To study the impact of excitons at QD excited states on the emission of bioconjugated QDs, the PL spectra were measured at different UV light (325nm) excitation intensities. The PL spectra of 655N QDs kept a Gaussian shape of PL band (1.90 eV) at all excitation intensities (Figure 6a). The full width at half maximum (FWHM) of PL band at the first increases with raising excitation intensities owing to the enlargement of the number of excited

http://dx.doi.org/10.5772/60821

QDs and their size distribution. Then the FWHM saturates at higher excitation intensities (Figure 6c, curve 1).

The PL spectra of bioconjugated QDs represent a set of PL bands: (i) PL band (I) with a peak at 2.10 eV connected with QD core emission; (ii) PL band (II) at 2.64 eV, apparently, is related to PBS emission; and (iii) PL band (III) with the peak at 2.78 eV (Figure 6b).

The high-energy PL band III is attributed to a CdSeS alloy appeared at the CdSe/ZnS interface [31]. The confirmation of the existence of such alloy has been obtained at the Raman scattering study in CdSe/ZnS QDs (see Figure 5). The formation of high-energy tails of PL band I together with increasing the PL band II and III intensities have been detected by raising the excitation light power (Figure 6b). Simultaneously, the intensity of a low-energy part of band I increases versus excitation power due to the increasing excited QD numbers and QD size distribution, as it has been seen in nonconjugated QDs. The FWHM of band I in bioconjugated QDs increases monotonously without saturation versus excitation intensity (Figure 6c, curve 2). This study has shown that the PL band I intensity increases with excitation power owing to the increasing emission of excitons localized at the excited states in bioconjugated QDs. The mentioned effect can explain the asymmetric shape of band I and the increasing FWHM (Figure 6c, curve 2) in bioconjugated QDs. Note that the exciton emission via excited states cannot explain "blue" shift (~200 meV) in the PL band I peak and appearing the PL band III in the PL spectra of QDs bioconjugated to anti-IL-10 Abs.

3.2. CdSe/ZnS QDs bioconjugated to HPV E7 and PRV Ab

The PL spectra of CdSe/ZnS QDs with emission 605 nm and 655 nm nonconjugated and bioconjugated to PRV and HPV E7 antibodies have been presented in Figures 7 and 8, respectively. The PL spectra of QDs in a nonconjugated state are characterized by the one Gaussian shape PL band peaked at 2.05 eV (Figure 7a) and 1.90 eV (Figures 7b and 8a) and related to exciton emission in corresponding CdSe cores. The PL spectra of bioconjugated QDs have changed essentially: the core PL band shifts into the high-energy spectral range ("blue" shift). Simultaneously, the PL intensity of core emission decreases at the bioconjugation, its half width increases, and the shape of PL band becomes asymmetric with the essential high-energy tails (Figures 7 and 8).

As we have shown above, the processes of oxidation, the CdSe material degradation, or the appearance of elastic strains have been not realized at the bioconjugation of QDs [31, 42]. The "blue" energy shift of PL bands in bioconjugated QDs can be assigned to the emission of HPV E7 or PRV antibodies or PBS at high-energy UV excitation and/or the emission of excitons localized at the excited QD states.

The PL spectra of HPV E7 Ab, PRV Ab, and PBS have been studied at UV excitation as well (Figure 9). As it is clear from Figure 9, the PL spectra of antibodies and PBS are characterized by PL bands in the spectral range of 2.0-3.2 eV. The intensity of PL band in the spectral range 2.0-3.2 eV related to PBS is five- or eightfold smaller than the intensity of PL band related to antibodies. Simultaneously, the intensity of PL band related to the antibodies 10-fold smaller than the PL intensity of CdSe/ZnS QD emission at the UV excitation. Thus, we can conclude

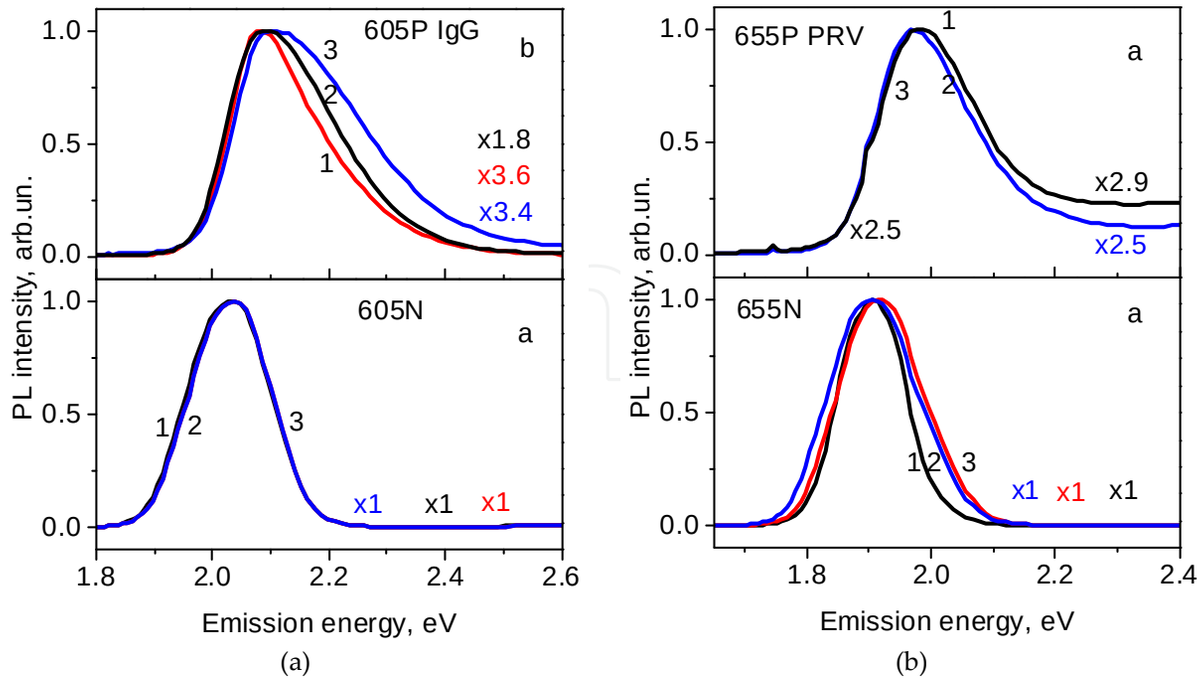

Figure 7. (a). Normalized PL spectra of three different 605N (a) and 605P-PRV (b) QD samples measured at 300 K. Numbers at the curves (×1, ×1.8, ×3.4, and ×3.6) indicate on the multiplication coefficients used at the normalization. (b). Normalized PL spectra of three different 655N (a) and 655P-PRV (b) QD samples measured at 300 K. Numbers at the curves (×1, ×2.5, and ×2.9) indicate on the multiplication coefficients used at the normalization.

as well that the "blue" energy shift of PL spectra in bioconjugated QDs does not connect with the emission of HPV E7 Ab, PRV Ab or PBS.

To study the role in the emission of excitons, localized at QD excited states in bioconjugated QDs, the PL spectra were measured at different excitation light intensities (Figure 8a, b). The PL spectra of nonconjugated 655N QDs kept the Gaussian shape of core PL band (1.90 eV) for all excitation intensities used (Figure 8a). The FWHM of this PL band at the first increases versus excitation intensity, due to raising the excited QD numbers and QD size distribution, and then the FWHM saturates at higher excitation intensities (Figure 8c, curve 1).

The PL band intensity in QDs, bioconjugated to HPV E7 Abs, increases versus excitation light power together with the formation of high-energy tails (Figure 8b). The PL band intensity at a low-energy side increases owing to rising the excited QD numbers and QD size distribution by the same way as in nonconjugated QDs. The FWHM of PL band in bioconjugated QDs increases monotonously versus excitation intensity without the saturation effect (Figure 8c, curve 2). Thus, the PL band intensity at a high-energy side increases versus excitation light power due to raising the role of exciton emission via excited states in bioconjugated QDs. This effect can explain an asymmetric shape of PL bands and increasing the FWHMs (Figure 8c, curve 2) in bioconjugated QDs. However, the emission of excitons localized at the excited QD states cannot explain shifting the main PL peak to higher energy in the PL spectra of bioconjugated CdSe/ZnS QDs.

http://dx.doi.org/10.5772/60821

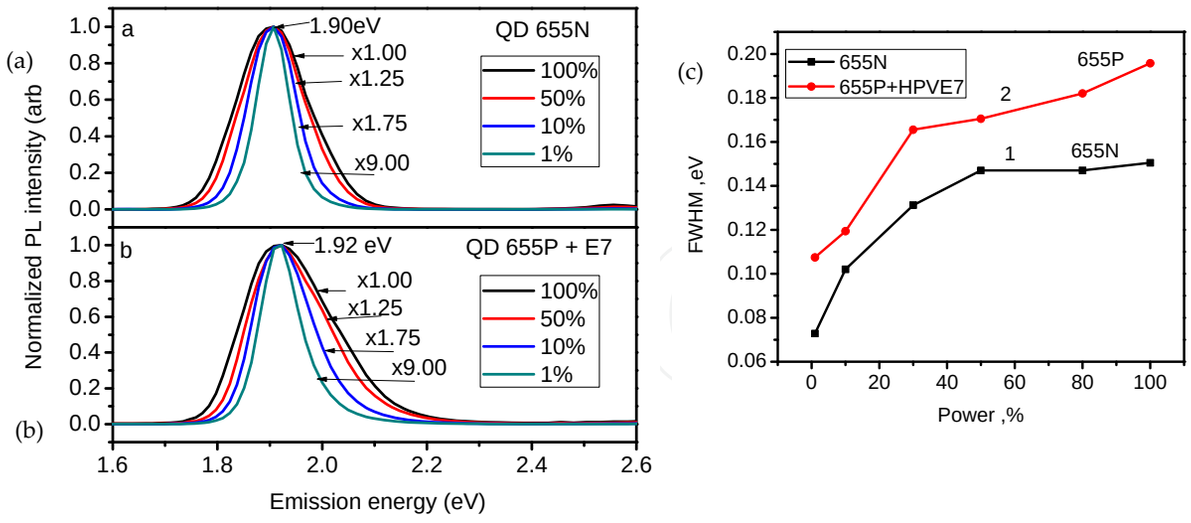

Figure 8. (a,b). Normalized PL spectra of 655N (a) and 655P-HPV E7 (b) QD samples measured at 300 K at the excitation intensities 100%, 50%, 10%, and 1%. The excitation intensity of 100% corresponds to 76 mW. (c). The FWHM variation of PL bands in 655N (1) and 655P-HPV E7 (2) QDs versus excitation light power. 100% corresponds to the power 76 mW.

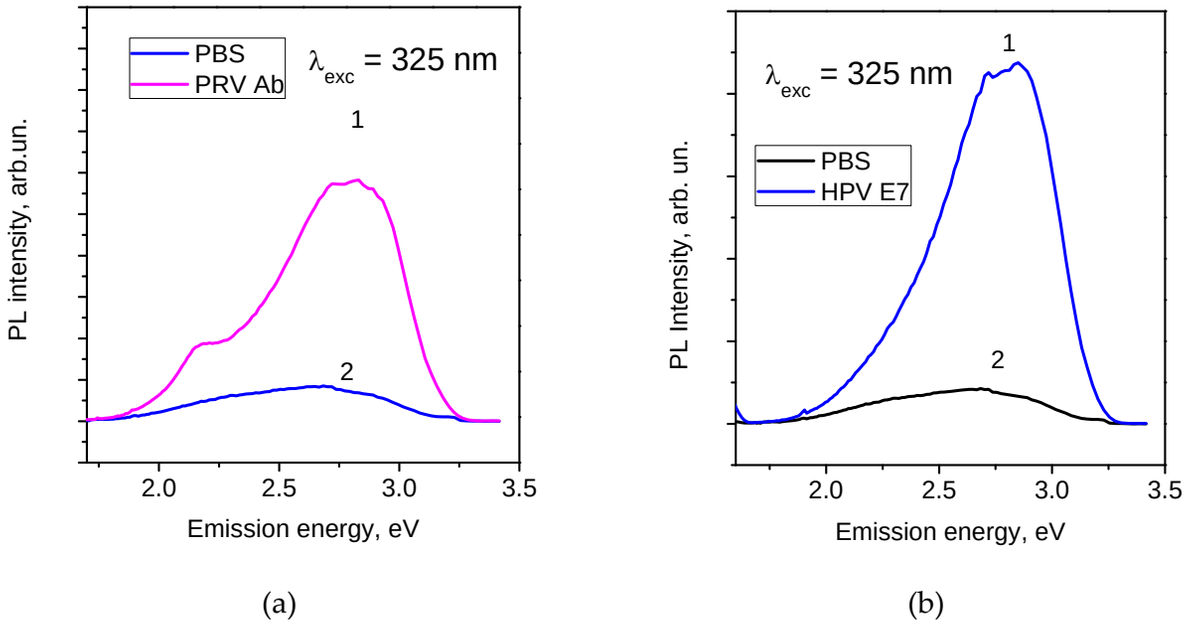

Figure 9. (a)PL spectra of PRV Ab (1) and PBS (2) without QDs. (b) PL spectra of HPV E7 Ab (1) and PBS (2) without QDs.

4. Discussion of the CdSe/ZnS QD bioconjugation

The experimental results presented above have shown that the influence of exciton emission via excited QD states or the emission of antibodies and PBS as well as the oxidation or degradation processes in QD cores can be avoided from the consideration as the reasons of "blue" PL peak shift at the QD bioconjugation. Let us discuss other reasons for the PL

energy shift at the bioconjugation of QDs to antibodies. These factors could be assigned to (i) the quantum-confined Stark effect stimulated by the charge of antibodies [43, 44], (ii) the quantum-confined effect related to the shift of QD energy levels and stimulated by the change of electric potential at the QD surface [45], or (iii) decreasing the effective QD size in bioconjugated QDs [46].

The Stark effect is shifting and splitting of energy levels in atoms and molecules due to the presence of external electric field. The Stark shift of energy levels, ΔE, as a function of electric field, ξ, can be presented as a sum of linear (first order Shark effect) and quadratic (second order Stark effect) functions of an electric field: $\Delta E = \mu_{QD} \xi + 0.5 \alpha_{QD} \xi^2 + ...$, where E is an energy of optical transition, and μ_{QD} and α_{QD} are projections of excited-state dipole and polarizability, respectively, along the electric field [43, 44]. This relation includes both the polar and polarizable parts of emitting state. Actually, the Stark shift in the emission of QD ensembles was found earlier to be purely quadratic versus applied electric field [39]. The dependences of the quantum-confined Stark shift versus QD sizes and electric fields in the CdS, CdSSe, and CdSe QDs were studied theoretically [44] and experimentally [43] in the early 90th. Only the "red" Stark energy shift was predicted theoretically for CdS and CdSSe QD ensembles at applying an external electric field [44]. Thus, we can conclude that the quantum-confined Stark effect could not explain the observed experimental "blue" energy shift of PL bands at the QD bioconjugation to studied antibodies.

Another reason for the "blue" shift of PL peak in bioconjugated QDs can be connected with the change of potential barrier at the surface of QDs bioconjugated to the charged antibodies. The position of energy levels in QDs for the strong quantum-confined regime depends on the value of potential barrier [45]. It was shown that the impact of a finite potential barrier on the electron-hole energy states increases with decreasing the dot radius. The lower potential barrier reduces and higher potential barrier increases the energy levels and these changes are more relevant for high-energy states [45]. However, the comparison of the PL spectrum transformation presented in Figures 2 and 3 or Figure 7a, b has shown that the value of "blue" PL energy shift at the QD bioconjugation to anti-IL-10 or PRV Abs is more essential for QDs with the biggest sizes (6.4 nm) and emission at 655 nm. Thus, the "blue" PL band energy shifts at the CdSe/ZnS QD bioconjugation to antibodies do not connect with the variation of the potential barrier at the QD surface.

The other reason for the "blue" shift of QD energy levels at the quantum-confined condition, owing to decreasing the effective QD size in bioconjugated QDs, was considered by Torchynska et al. [46]. When QD is bioconjugated, its energy balance changes very much. The energy variation comes from the fact that the attachment of biomolecules to the external QD surface will result in the generation of van der Waals forces. The extra charge attached to the exterior shell will form a blocking electric field, which "truncates" the effective volume of QDs (Figure 10). In this situation, it is natural to expect energy varying of emitted light. At the same time, the stronger confinement will produce a blue shift of the QD emission spectrum.

The question about the accurate calculation of the truncated volume is a complicated one. For a point charge, the equipotential surfaces will be spheres, which will make the blocked volume corresponding to a spherical segment. The remaining effective volume will lose its spherical

http://dx.doi.org/10.5772/60821

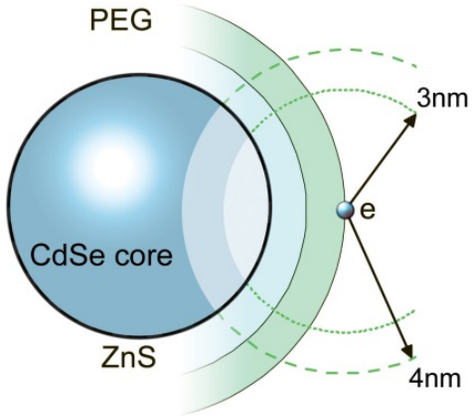

Figure 10. A schematic depiction of CdSe/ZnS QD with the 6.4 nm CdSe core, encased in the ZnS and poly-ethylene glycol (PEG) protective shells. A charge generated upon bioconjugation is shown attached to the PEG shell to the right. We consider two radii of the blocking sphere of d = 3 and 4 nm, respectively.

shape. We proposed to approximate it with a cylinder with a height c and a circular base of the diameter a. The Schrödinger equation for such system was solved using the mirror boundary conditions [46, 47], providing the ground state energy relative to the material band gap [47]:

$$E_{GSc} - E_g = \frac{h^2}{2m}\left(\frac{0.268}{a^2} + \frac{0.25}{c^2}\right) \quad (1)$$

The parameters of a cylinder can be estimated for different strength of the blocking field. We consider two cases with the blocking field extending for the distance d = 3 and 4 nm from the charge attached to the protective PEG layer covering nanoparticle (Figure 9). For these cases, the parameters of the effective cylinder are as follows: a = 1.6 R, c = 1.55 R (for 4 nm blocking radius) and a = 1.65 R, c = 1.6 R (for 3 nm blocking radius), where R = 3.2 nm is the radius of the CdSe core of the particle. Using these values, one can obtain the expressions for the ground state of conjugated nanoparticle with 4 nm blocking [46]:

$$E_{GS_c} - E_g \approx \frac{h^2}{9.6mR^2} \quad (2)$$

and also for conjugated nanoparticle with 3 nm blocking distance [46]:

$$E_{GSc} - E_g \approx \frac{h^2}{11.1mR^2} \quad (3)$$

In a real system, the absorbed energy that triggered the formation of an exciton can be partially dissipated, so that the peak of PL spectra will occur at lower energy, producing Stokes shift

E_{St}. Therefore, the total blue shift observed in the system can be defined as a ratio between peak positions of a bioconjugated sample $h\nu_c$ versus nonconjugated sample $h\nu_0$:

$$\frac{E_{GS_c} - E_g}{E_{GS_0} - E_g} = \frac{h\nu_c + E_{St} - E_g}{h\nu_0 + E_{St} - E_g} \tag{4}$$

Using the experimental data shown in Figure 3, one can see that $h\nu_0$ = 1.89 eV and $h\nu_c$ = 2.08 eV; the typical Stokes shift is E_{St} = 56.0 meV [48]. Using the band gap E_g = 1.74 eV for the bulk CdSe at 300 K [49], one can obtain the ratio for the experimental shift equal to 2.16 from equation (4). The ratios calculated with Eqs. (1), (2), (3), and (4) are 3.30 (for blocking distance d = 4 nm) and 2.88 (for d = 3 nm), which is considerably close to the experimental value in view of simplifications made in treating the truncation of nanoparticle's core volume.

Thus, we have proposed to use the mirror boundary condition for simplifying solution of the Schrödinger equation for a spherical CdSe/ZnS core/shell QDs. It was shown that the "blue" shift in the PL spectrum observed in the experiment with bioconjugated QDs can be explained by the attachment of a charge deals with the antibody to the exterior shell of QDs, blocking away a fraction of core's volume. Representing the truncated effective part of core as a cylinder, we obtained a blue shift values with a considerable accuracy in relation to the experimental data. Thus, the "blue" energy shift of PL spectrum in the bioconjugated CdSe/ZnS QDs has been attributed to the electronic quantum-confined effects stimulated by the charged antibodies.

5. The bioconjugation study of CdSeTe/ZnS QDs

5.1. CdSeTe/ZnS QDs bioconjugated to anti-IL-10 Ab

The PL spectra of CdSeTe/ZnS QDs for the nonconjugated (800N) and bioconjugated (800P+IL-10) states are shown in Figure 11. The PL spectrum of 800N QDs is characterized by Gaussian shape PL band with a peak at 1.59-1.60 eV (Figure 11, curves 1 and 2) connected with exciton emission in CdSeTe cores. The PL peak shifts to higher energies ("blue" shift) up to 1.90 eV (Figure 11, curves 3 and 4), and the shape of PL bands becomes asymmetric with low-energy shoulders (at 1.75 eV) in the PL spectra of bioconjugated QDs (Figure 11, curves 3 and 4). Simultaneously, the PL intensity of QDs decreases in the case of the bioconjugation to anti-IL-10 Ab (Figure 11, curves 3 and 4).

The PL spectra of anti-IL-10 Ab and PBS have been measured at the UV light excitation early (Figure 4). The PL spectrum of anti-IL-10 Ab is characterized by the PL band with a peak at 2.21 eV and a small PL shoulder in the range 2.3-3.0 eV (Figure 4, curve 1). The intensity of the PL band related to PBS (Figure 4, curve 2) is 15-fold smaller than the emission intensity of 2.21 eV PL band connected with anti-IL-10 Abs. Note that the 2.21 eV PL band intensity in anti-IL-10 Abs is 10-fold smaller than the emission intensity of excitons in CdSeTe/ZnS QDs at UV

http://dx.doi.org/10.5772/60821

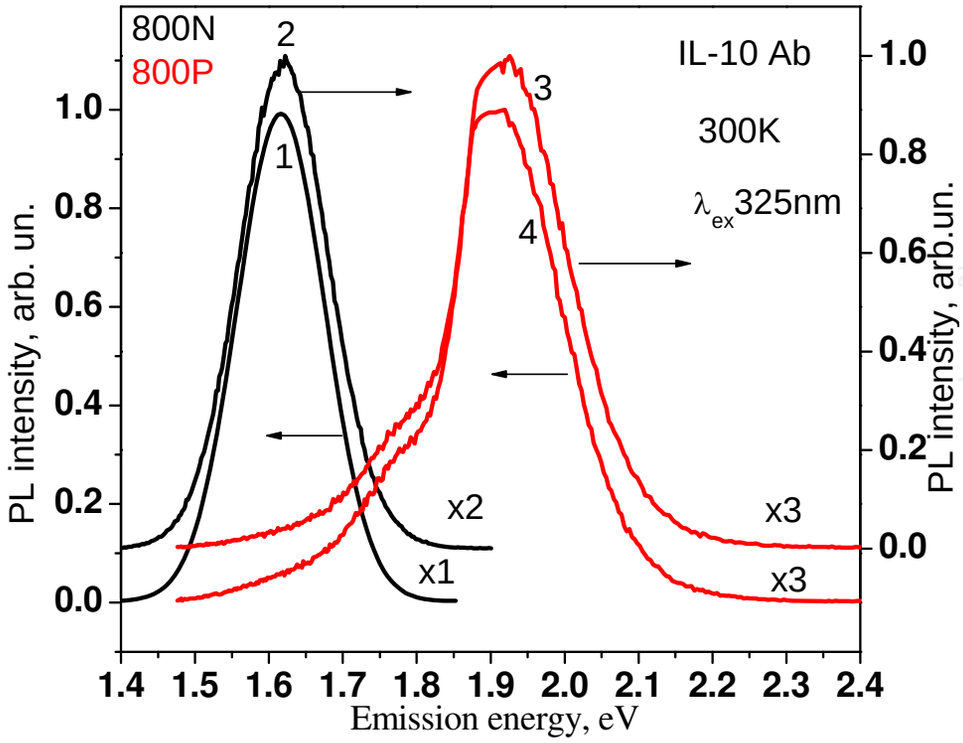

Figure 11. Normalized PL spectra of two 800N (curves 1 and 2) and two 800P+ IL-10 (curves 3 and 4) QD samples at 300 K. PL spectra are shifted along *y* axis to prevent their overlapping. Numbers (x1, x2, x3) indicate the multiplication coefficients used at the normalization. Excitation light wavelength is 325 nm.

light excitation (Figure 11). Thus, the new PL bands peaked at 1.75 and 1.90 eV that appeared in the PL spectra of bioconjugated QDs do not related to the emission of anti-Il-10 Abs or PBS.

To study the impact of the excitation quanta energy on the shape of PL bands, the PL spectra of nonconjugated and bioconjugated QDs have been measured using the different excitation wavelengths of 532 nm, 488 nm, and 325 nm (Figure 12). The difference in PL intensities is related to the power of lasers used, but the shape of PL bands in the nonconjugated and bioconjugated QDs is similar. Note that the PL intensity of QD emission is higher at the UV excitation (325 nm).

The Raman scattering spectra of CdSeTe/ZnS QDs are investigated as well. The Raman spectrum of nonconjugated CdSeTe/ZnS QDs represents a complex Raman peak of QDs at 202.5 cm^{-1} and the Raman peak at 519.6 cm^{-1} connected with the first-order Raman scattering involving optic phonons in the Si substrate (Figure 13a). The Raman peak of QDs is a superposition of two Raman peaks at 191.2 and 202.5 cm^{-1} (Figure 13a), which correspond to the LO phonons in the $CdSe_{50}Te_{50}$ core and $CdSe_{80}Te_{20}$ core's cover layer [31, 50]. In addition, the Raman spectrum represents two peaks at 177.0 and 280 cm^{-1}. The peak at 177.0 cm^{-1} could be assigned to a surface phonon (SP) in QD cores [6]. The Raman peak at 280 cm^{-1} is probably due to the CdZnSeS alloy that appears at the CdSeTe/ZnS interface at the temperature of ZnS shell growth [6, 50-52].

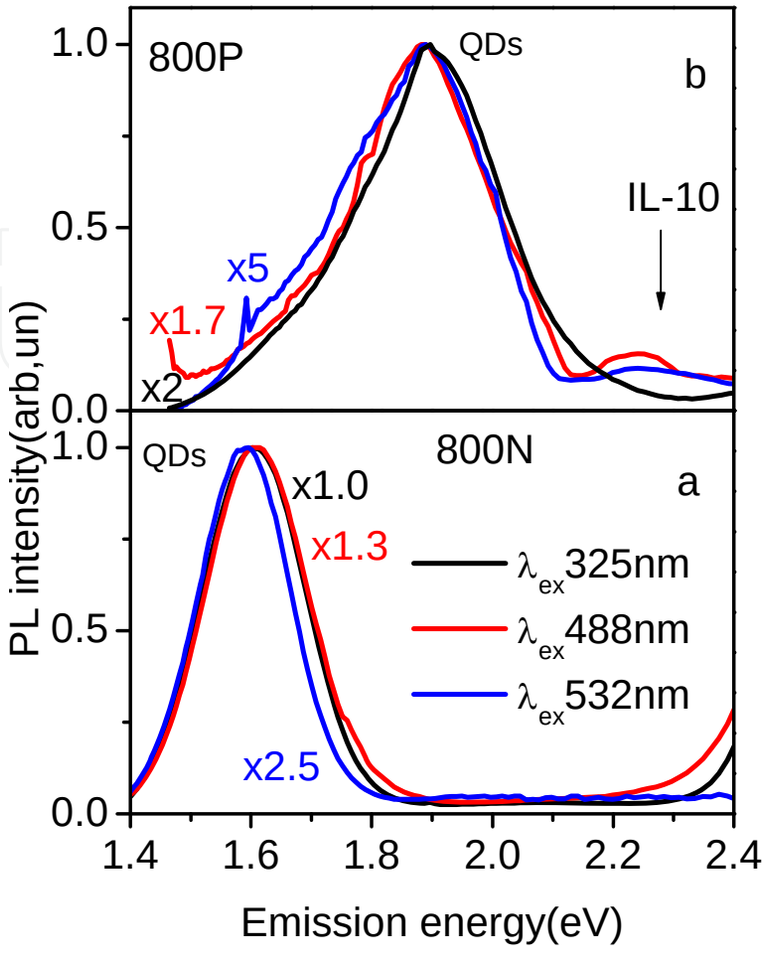

Figure 12. PL spectra of 800N (a) and 800P+ IL-10 (b) CdSeTe/ZnS QDs measured at 300 K and excited by the light with wavelengths: 532 nm (1), 488 nm (2), and 325 nm (3).

The Raman scattering investigation shows (Figure 13a, b) that the Raman peaks related to the LO phonons in the double CdSeTe core and in the alloy at the interface did not vary at the QD bioconjugation. This fact testifies that the "blue" PL energy shift in bioconjugated CdSeTe/ZnS QDs (Figures 11 and 12) has been not connected with compressive strains or with the degradation of CdSeTe QD core owing to core/shell intermixing or core oxidation at the QD bioconjugation.

5.2. CdSeTe/ZnS QDs bioconjugated to the HPV and PRV antibodies

Normalized PL spectra of nonconjugated and bioconjugated CdSeTe/ZnS QDs have been presented in Figures 14, 15, and 16 for the different antibodies used: (i) mouse monoclonal anti-HPV E7 Ab, (ii) mouse monoclonal HPV E6 Ab, and (iii) pseudorabies virus (PRV) Ab.

QD emission spectra in nonconjugated state are characterized by the two Gaussian shape PL bands. The main PL band (I) with a maximum at 1.57-1.60 eV (Figures 14-16, curve 1) is connected with exciton emission in the CdSeTe core. The small intensity PL band (II) with a

http://dx.doi.org/10.5772/60821

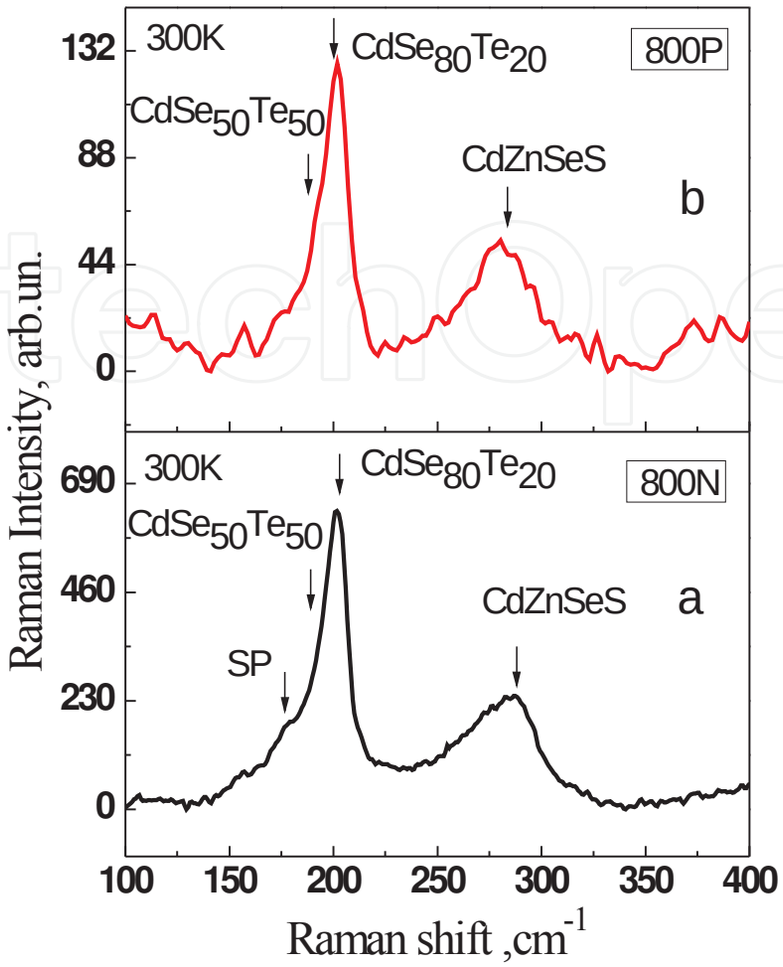

Figure 13. Raman scattering spectra of 800N (a) and 800P+ IL-10 (b) QDs.

peak at 2.50 eV is attributed to exciton emission in the intermediate alloy CdZnSeS layer at the core/shell interface [50-52]. This intermediate layer was introduced at the process of QD growth with the aim to decreasing the mismatch between the CdSeTe and the ZnS crystal lattices. The PL intensity of 2.50 eV band varies owing to the variation, apparently, a volume of intermediate alloy layers in the different QD ensembles (Figures 14-16). The small intensity PL band at 2.50-2.90 eV (Figure 15) can be connected with the emission of PBS (see Figures 4 and 9) that exists in the nonconjugated QD ensembles as well.

The main PL peak (I) shifts to higher energy in the PL spectra of bioconjugated QDs up to: 1.881 eV (Figure 14, curve 2), 1.887 eV (Figure 15, curve 2), or even 1.937 eV (Figure 16, curve 2). Simultaneously, the PL band shape becomes asymmetric with essential low-energy shoulders. The analysis has revealed that the main PL band in bioconjugated QDs is complex and can be represented by a superposition of two PL bands (Figure 15, curves 3 and 4): the low-energy band with a peak at 1.60 eV and the high-energy band centered at 1.887 eV in Figure 15. At the same time, the PL intensity of main PL band I decreases and the additional PL band appears in the spectral range 2.2-3.0 eV.

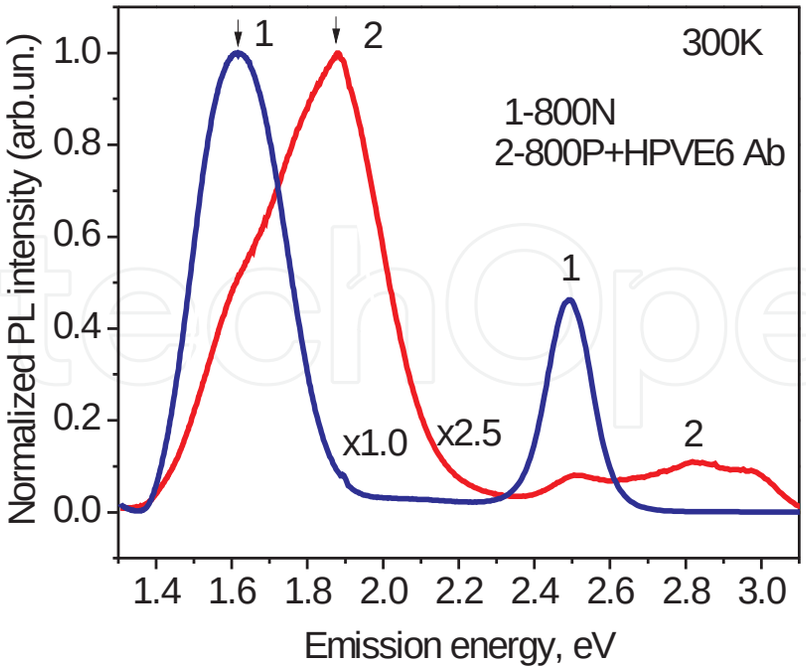

Figure 14. Normalized PL spectra of nonconjugated 800N (1) and bioconjugated 800P (2) QDs to HPV E6 Ab measured at 300 K. Numbers at the curves (×1.0 and ×2.5) present the multiplication coefficients used at the normalization of experimental PL spectra.

6. Discussion of the CdSeTe/ZnS QD bioconjugation

Let us discuss again the physical reasons of PL spectrum transformation at the QD bioconjugation to antibodies. As we mentioned above, these reasons can be related to (i) the emission of antibody molecules or PBS at UV excitation; (ii) the compressive strain applied to QDs at the bioconjugation [33]; (iii) the compound material degradation owing to core/shell intermixing [53] or oxidation [32] at the QD bioconjugation; (iv) the quantum-confined Stark effect [43, 44], stimulated by electric charges of antibodies; (v) the dominated emission of excitons localized at the excited QD states; (vi) the change of energy band profile at the application of electric field of charged Abs; and (vi) the quantum-confined effect owing to the shift of QD energy levels stimulated by the change of potential barrier at the QD surface [45] or by decreasing the effective QD size in bioconjugated QDs [46]. To make the decision concerning the most probable physical reasons of the PL transformation in CdSeTe/ZnS QDs, let us analyze all of these factors in details.

(i) The emission of HPV or PRV antibodies and PBS can be excited together with QD emission at the PL excitation by UV light (325 nm). The PL spectra of pure HPV and PRV antibodies, and PBS without QDs have been investigated (Figure 17).

The wide emission bands have been detected in the spectral range 2.0-3.2 eV in PL spectra of both the antibodies and PBS (Figure 17). The PL intensity of PBS emission is 50-fold smaller, and the PL intensities of antibody's emissions are 5- or 10-fold smaller in comparison with the PL intensity of the main PL bands I in bioconjugated CdSeTe/ZnS QDs. Thus, the emission of

http://dx.doi.org/10.5772/60821

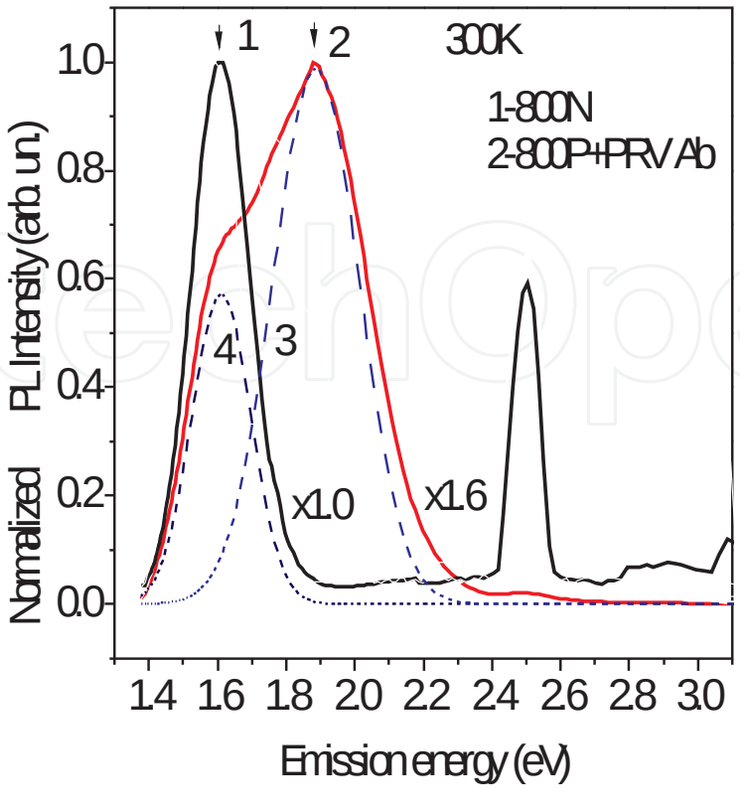

Figure 15. Normalized PL spectra of nonconjugated 800N (1) and bioconjugated 800P QDs (2) to PRV Ab measured at 300 K. Numbers (×1.0 and ×1.6) present the coefficients used at the normalization of PL spectra. Dashed curves (3 and 4) show the deconvolution of curve 2 on two PL bands.

antibodies or PBS at the high-energy UV light excitation cans influent only on the shape of high-energy tails in PL spectra of bioconjugated QDs. This impact is seen clearly in Figures 14, 15, and 16 (curve 2), where the high-energy PL band appears in the spectral range 2.2-3.2 eV.

(ii-iii) If the compressive strain appears at QD bioconjugation, the Raman peaks has shift in Raman spectra in comparison with those for nonconjugated QDs. The Raman scattering spectrum of nonconjugated CdSeTe/ZnS QDs represents a complex Raman peak of QDs at 202.5 cm^{-1} and another Raman peak at 519.6 cm^{-1} related to the Si substrate (Figures 13a and 18a).

The QD peak is a superposition of Raman peaks at 191.2 and 202.5 cm^{-1} (Figure 18a), which correspond to Raman scattering involving the LO phonons of the $CdSe_{50}Te_{50}$ core and $CdSe_{80}Te_{20}$ core's cover layer [31, 50]. The detailed estimations of material compositions in the double CdSeTe QD core on the base of Raman peak analysis were published earlier by Quintos Vazquez et al. [31]. The Raman spectrum demonstrates as well the peak at 280 cm^{-1}, which can be assigned to light scattering by LO phonons in the CdSeZnS intermediate alloy layer. The Raman peak at 406 cm^{-1} is related to two-phonon Raman scattering in the CdSeTe core [50]. The intensity of Raman signals in bioconjugated CdSeTe/ZnS QDs increases in comparison with those in nonconjugated QDs [54]. This effect was attributed early to the surface-enhanced

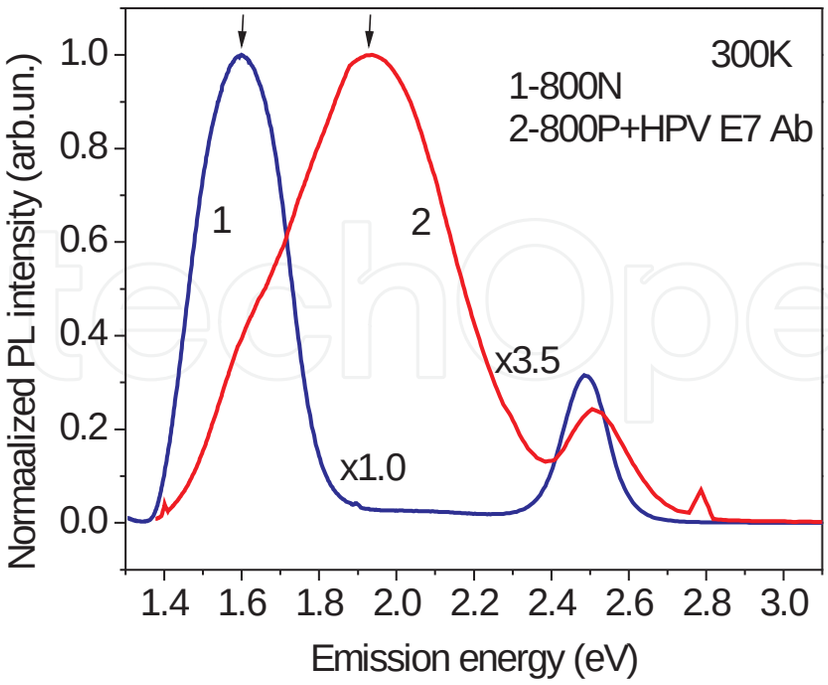

Figure 16. Normalized PL spectra of nonconjugated 800N (1) and bioconjugated 800P QDs (2) to HPV E7 Ab at 300 K. Numbers at the curves (×1.0 and ×3.5) correspond to multiplication coefficients used at the normalization of experimental PL spectra.

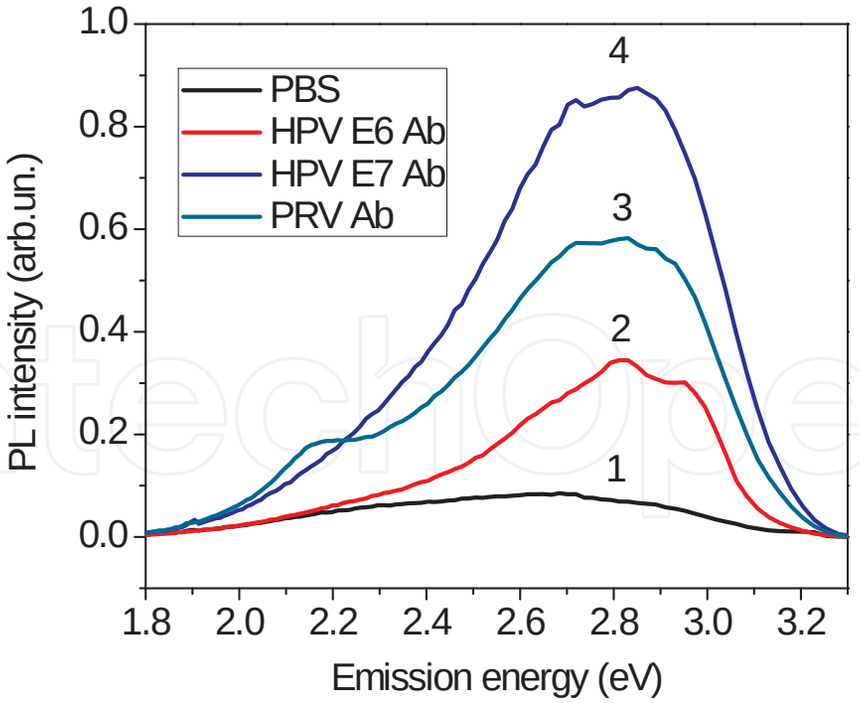

Figure 17. PL spectra of PBS (1), HPV E6 Ab (2), PRV Ab (3), and HPV E7 Ab (4) without QDs.

http://dx.doi.org/10.5772/60821

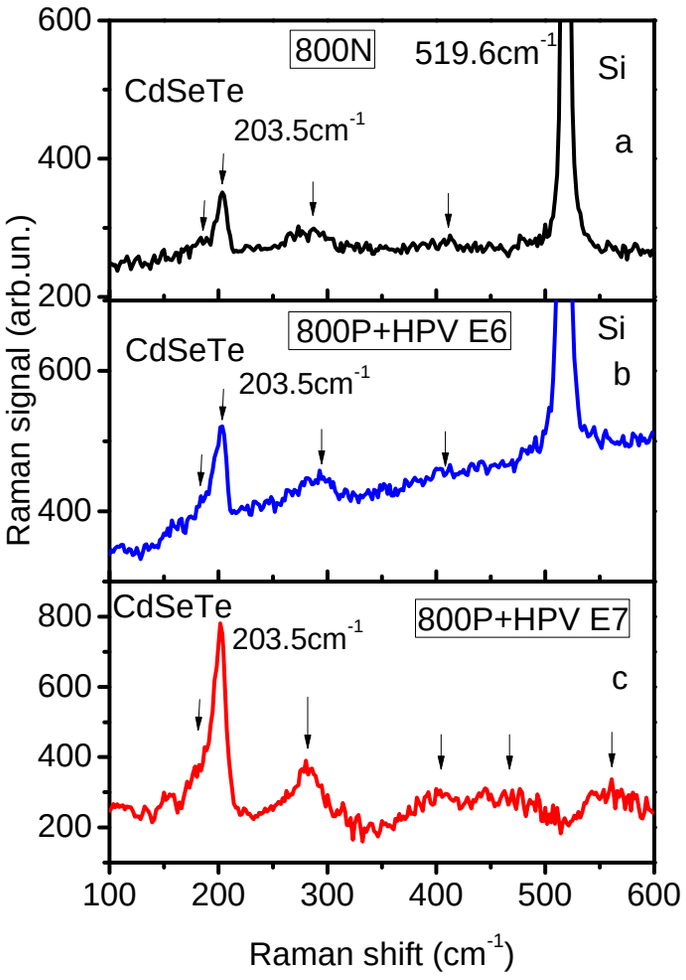

Figure 18. Raman scattering spectra of nonconjugated 800N (a) and bioconjugated 800P (b, c) QDs to HPV E6 (b) and HPV E7 (c).

Raman scattering (SERS) [22, 39, 54] due to the interaction of the electromagnetic field of excitation light with the electric charges (dipoles) of antibodies. The realization of the SERS effect at Raman scattering in bioconjugated QDs testifies that the antibodies have the electric charges.

The SERS effect is responsible for appearing the low-intensity Raman peaks (463 and 580 cm^{-1}) in Raman spectra of bioconjugated QDs (Figure 18c). These Raman signals are related to the Si substrate and were assigned early to scattering involving TO phonons (463 cm^{-1}) and the combination of TA and TO phonons at the X direction in the Si Brillouin zone [36]. The Raman scattering study shows (Figure 18b, c) that the positions of Raman peaks in Raman spectra of the double CdSeTe core and intermediate CdSeZnS layer have not been varied at the CdSeTe/ZnS QD bioconjugation. Permanent positions of Raman signals in QDs testify that the bioconjugation process has not connected with the compressive strains to QDs, with the compound degradation owing to core/shell intermixing or the QD core oxidation at the bioconjugation.

(iv) The quantum-confined "red" Stark energy shift was predicted theoretically for emission in the ensembles of CdS or CdSSe QDs [43, 44]. The quantum-confined Stark effect can be avoided from our discussion as well because the "blue" PL energy shift is detected in studied CdSeTe/ZnS QDs at the bioconjugation.

(v) To analyze the role of excitons bounded at the excited states in the CdSeTe core, the dependence of PL spectrum transformation versus excitation light intensities has been studied (Figure 19a-c). As it is clear from Figure 19a, the shape of PL bands in nonconjugated CdSeTe/ZnS QDs (800N) has not changed at varying the excitation light intensities.

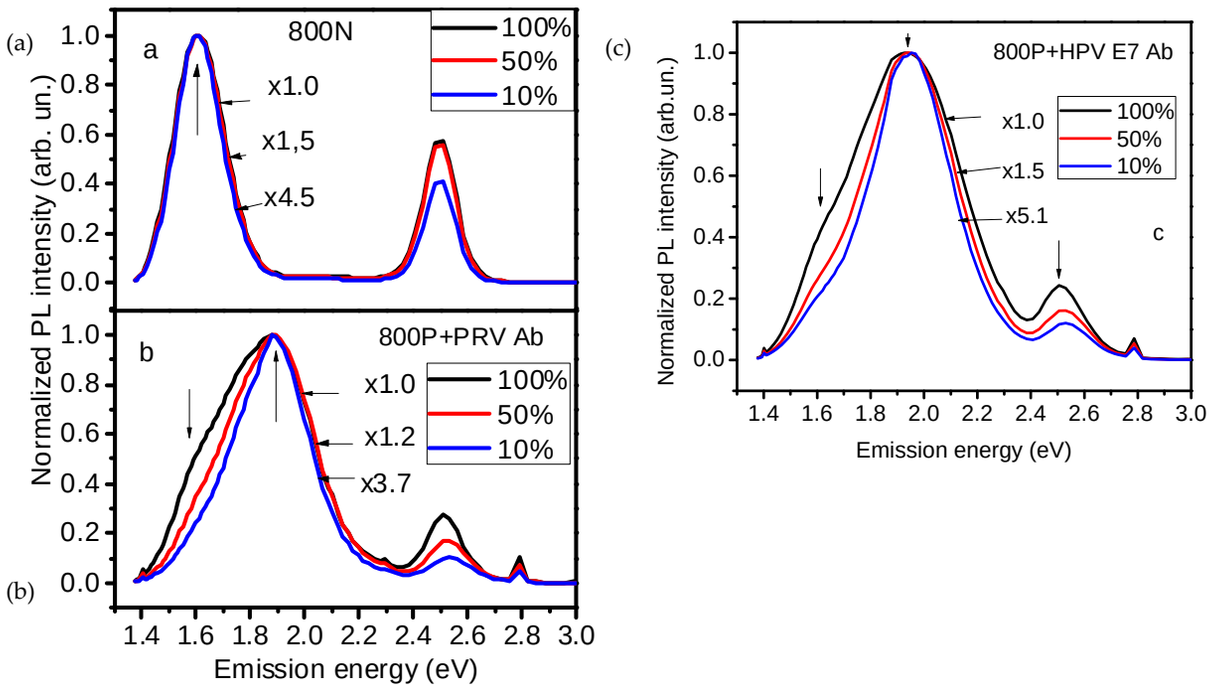

Figure 19. Normalized PL spectra of nonconjugated (a) and bioconjugated QDs to PRV Ab (b) and to HPV E7 Ab (c) measured at different excitation light powers at 300 K.

Meanwhile, the shape of the PL spectra of bioconjugated QDs varies versus excitation light power (Figure 19b, c). The PL intensity decreases mainly in the low-energy (1.60 eV) and high-energy (2.50 eV) ranges that have been seen clearly. The mentioned PL bands do not connect with the emission of excitons localized at the excited states in the CdSeTe core. Thus, the emission of excitons localized at the excited states in bioconjugated CdSeTe/ZnS QDs is not responsible for the transformation of PL spectra versus excitation light power.

(vi) Let us consider the energy band diagram of CdSeTe/ZnS QDs with the aim to analyze the varying energy band profile at the bioconjugation. The energy diagram of the double core CdSeTe/ZnS QDs with emission at 800 nm was calculated early by Quintos Vazquez et al. [31]. The band gaps and electronic affinities for the $CdSe_{50}Te_{50}$, $CdSe_{80}Te_{20}$, and ZnS bulk crystals [31, 55] have been represented in Figure 20.

http://dx.doi.org/10.5772/60821

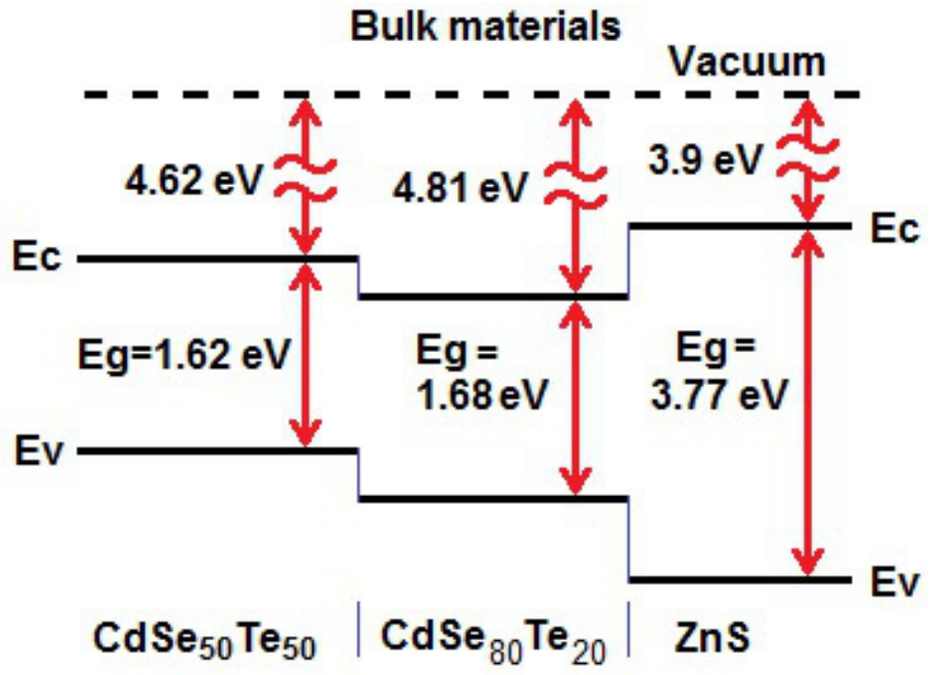

Figure 20. Energy band diagram for the CdSeTe alloys and ZnS bulk crystal.

To create the energy diagram of nonconjugated CdSeTe QDs (Figure 21), the variation of energy band gaps for the $CdSe_{50}Te_{50}$ core and $CdSe_{80}Te_{20}$ core cover layer with their sizes is estimated using the effective mass approximation model [31]. The big size of the double core/shell CdSeTe/ZnS QDs (emission, 800 nm) permits to apply the effective mass approximation approach [6].

The ground energy of electron-hole pairs and the energy of the first absorption transition are estimated as follows [56]:

$$E_{1S1S} = E_g + \frac{\hbar^2\pi^2}{2\mu\alpha^2} - 1.786\frac{e^2}{\varepsilon\alpha} - 0.248R_y \quad (5)$$

where E_g is the energy band gap of bulk material, α is a QD radius, μ is the reduced mass, $\mu^{-1} = m_e^{*-1} + m_h^{*-1}$, m_e* and m_h* are the effective masses of electrons and holes, and ε is the high-frequency permittivity. The term $\frac{e^2}{\varepsilon\alpha}$ in Eq. (5) describes the electron-hole Coulomb interaction, and the fourth term is a minor correction.

To analyze the energy band gap, the following parameters have been used for the bulk CdSe: E_g = 1.730 eV at 300 K, m_e* = 0.13 m_o, m_h* = 0.45 m_o, and the high-frequency permittivity ε = 8.2 [50, 51]. Using the parameters for the bulk CdTe: E_g = 1.50 eV at 300 K, m_e* = 0.11m_o, and m_h* = 0.35m_o [50, 57], the values of energy band gaps and effective masses for the bulk $CdSe_{0.8}Te_{0.2}$ and $CdSe_{0.5}Te_{0.5}$ alloys have been obtained by the linear interpolation. To estimate the position of PL excitation peaks connected with the electron-hole ground states in QD, the value of Stokes

shift is taken in account, which equals 50 meV [6]. Estimated energy band gaps for the $CdSe_{0.5}Te_{0.5}$ and $CdSe_{0.8}Te_{0.2}$ alloys have been used for the design of the energy diagram of the double core/shell QDs (Figure 21).

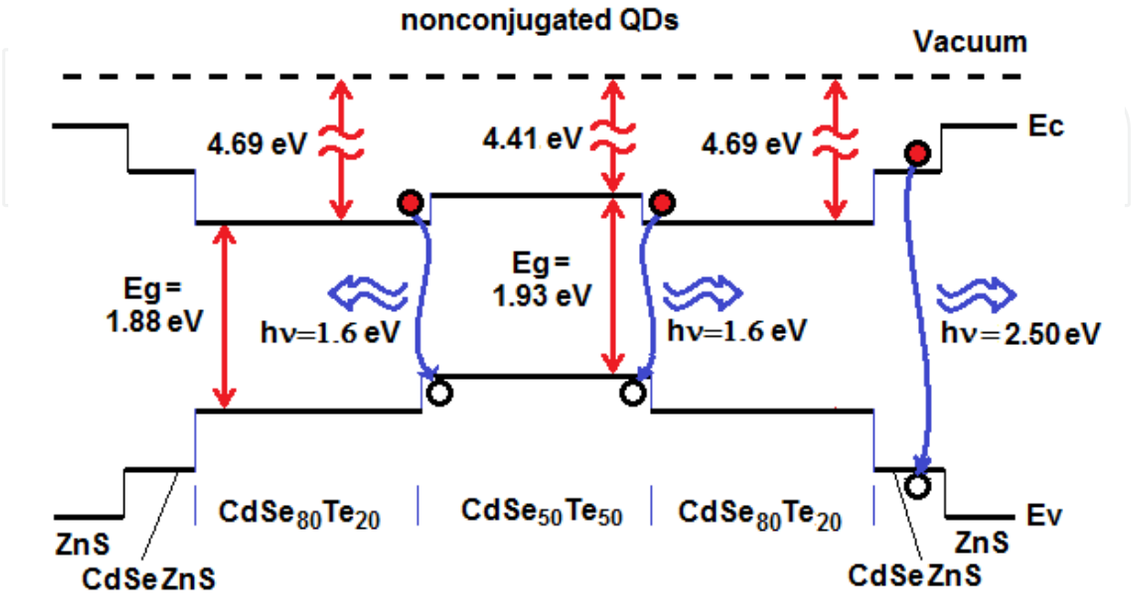

Figure 21. The energy band diagram of nonconjugated double core CdSeTe/ZnS QDs.

The energy band diagram of nonconjugated CdSeTe/ZnS QDs (Figure 21) explains the types of the optical transitions and emission energy of 1.60 eV detected in the PL spectra of nonconjugated QDs. As it is clear from Figure 21, owing to the type II quantum well ($CdSe_{80}Te_{20}$/$CdSe_{50}Te_{50}$/$CdSe_{80}Te_{20}$) in double core QDs, the wide band gap core and the core's covered quantum well layer with the energy band gaps of E_g = 1.93 and 1.88 eV, respectively, enable to emit IR emission with a PL peak at 1.60 eV in nonconjugated QDs (Figures 11, 14, 15, and 16). This 1.6-eV emission owes to the recombination of electrons, from the $CdSe_{80}Te_{20}$ conduction band, with holes localized in the $CdSe_{50}Te_{50}$ valence band (Figure 21).

To explain the PL band "blue" shift into the higher energy range (1.88-1.94 eV) in bioconjugated CdSeTe/ZnS QDs (Figures 11, 14, 15, and 16), let us to consider the transformation of band diagram at applying the external electric field of charged antibodies. In this case, the energy band profile varies as it is presented in Figure 22. Actually, in the bioconjugated QDs, the two types of optical transitions are possible: the recombination of excitons located at the ground states in the $CdSe_{50}Te_{50}$ core and/or the recombination of electrons, from the $CdSe_{80}Te_{20}$ conduction band, with holes localized in the $CdSe_{50}Te_{50}$ valence band (Figure 22).

The transformation of PL spectra versus excitation light intensities (Figure 19) has confirmed the proposed QD energy band diagrams. Actually, at low excitation light intensity, the recombination (1.88 eV) of excitons at the ground $CdSe_{50}Te_{50}$ core states dominates in the PL spectrum (Figure 22). At obtaining the last value (1.88 eV), the Stock shift of 50 meV is taken into account [6, 29, 30]. When excitation intensity increases, the indirect recombination

http://dx.doi.org/10.5772/60821

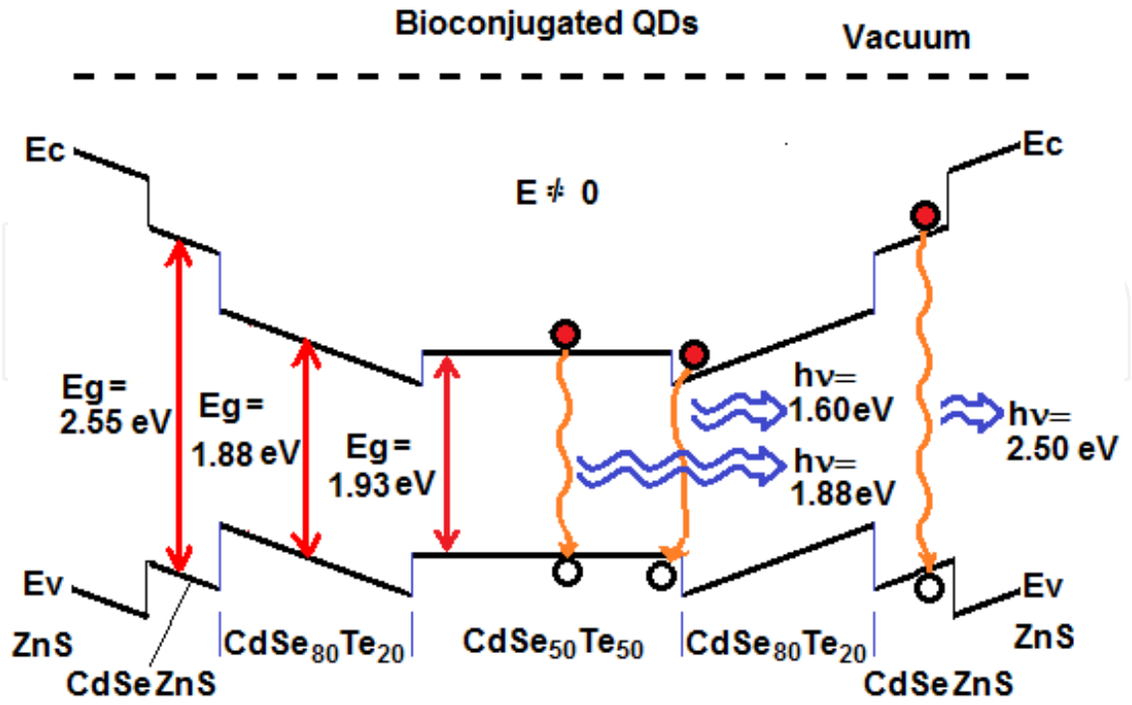

Figure 22. Energy band diagram of QDs bioconjugated to 800P+HPV E6 Ab.

transition (electrons from $CdSe_{80}Te_{20}$ with holes in $CdSe_{50}Te_{50}$) and exciton emission in the intermediate CdSeZnS layer can be realized. Hence, the energy band profile variation in the double core CdSeTe/ZnS QDs at the bioconjugation to charged antibodies permits to explain the PL spectrum peculiarities of bioconjugated QDs.

(vii) Finally, let us discuss the difference in PL band positions in CdSeTe/ZnS QDs bioconjugated to different antibodies (Figures 14-16, curve 2). The main PL peaks in bioconjugated QDs are as follows: 1.881 eV for 800P+HPV E6 Ab (Figure 14, curve 2), 1.887 eV for 800P+PRV Ab (Figure 15, curve 2), and 1.937 eV for 800P+HPV E7 Ab (Figure 16, curve 2). The difference in PL peaks can be related to the difference in electric potentials (potential barriers) at the surface of bioconjugated QDs. It is known that the position of energy levels in QDs, for the strong quantum confinement regime, depends on the value of potential barriers at the surface [45]. The comparison of PL intensities, detected for the pure antibodies (Figure 17), and the corresponding PL peaks in bioconjugated QDs (Figures 14-16, curve 2) have shown that the antibody HPV E7 with highest emission intensity (Figure 17, curve 4) stimulates the biggest PL band shift up to 1.937 eV (Figure 16, curve 2). The PL intensity, measured for the pure antibodies (Figure 17), depends on their concentrations in PBS. Thus, it is possible to conclude that the shift of PL spectra depends on a number of charged antibodies bioconjugated to CdSeTe/ZnS QDs [58]. Moreover, this PL shift increases by enlarging the antibody concentration in PBS. The potential barrier increasing at the QD surface has shifted the QD emission into the higher energy range owing to the shift of QD energy levels [58].

Thus, the PL spectrum transformation of CdSeTe/ZnS QDs, bioconjugated to studied antibodies, is related to the two effects: (i) the change of energy band profiles and (ii) the quantum-

confined effect owing to the shift of QD energy levels stimulated by the change of electric potentials (potential barrier) at the surface of QDs bioconjugated to charged antibodies. The potential barrier increasing has shifted the QD energy levels and QD emission into the higher energy range.

7. Conclusion

Photoluminescence, its excitation power dependence, and Raman scattering spectra have been studied in CdSe/ZnS and CdSeTe/ZnS QDs for the nonconjugated states and after the QD conjugation to the anti-IL-10, human papilloma virus, and pseudorabies virus antibodies. The QD bioconjugation to charged antibodies stimulates the "blue" energy shift of PL bands related to exciton emission in the CdSe or CdSeTe cores.

The "blue" energy shift of PL spectrum in bioconjugated CdSe/ZnS QDs has been attributed to the electronic quantum-confined effects stimulated by decreasing the effective QD size at its bioconjugation to charged antibodies. It was shown that the attachment of a charge, deals with the antibody, to the exterior shell of CdSe/ZnS QDs leads to blocking away a fraction of core's volume.

The energy band diagrams of CdSeTe/ZnS QDs in the nonconjugated and bioconjugated states have been designed, which permit to explain the types of optical transitions in QDs and their transformations at the QD bioconjugation. It is shown that the change of energy band profile and the "blue" shift of QD energy levels, owing to the change of potential barrier at the QD surface, are the dominant reasons of PL spectrum transformation in the double core CdSeTe/ZnS QDs conjugated to charged antibodies. A better understanding of the QD bioconjugation to specific antibodies is expected to produce the major advances in biology and medicine and can be a powerful technique for early medical diagnostics.

Acknowledgements

The work was partially supported by CONACYT (project 130387) and by SIP-IPN (projects 20140648 and 20150601), Mexico. The author would like to thank Dr. Janna Douda for the QD bioconjugation to antibodies and Dr. Jose Luis Casas Espinola for the PL measurements.

Author details

Tetyana V. Torchynska

Address all correspondence to: ttorch@esfm.ipn.mx

National Polytechnic Institute, ESFM, Mexico D.F., Mexico

References

[1] T. Jamieson, R. Bakhshi, D. Petrova, R. Pocock, M. Imani, A.M. Seifalian, Biomaterials 28, 4717 (2007).

[2] D. Gerion, W.J. Parak, S.C. Williams, D. Zanchet, C.M. Micheel, A.P. Alivisatos, J Am. Chem. Soc. 124, 7070 (2002).

[3] X.H. Gao, Y.Y. Cui, R.M. Levenson, L.WK. Chung, S.M. Nie, Nat. Biotechnol. 22, 969 (2004).

[4] Z. Liu, W.B. Cai, L.N. He, N. Nakayama, K. Chen, X.M. Sun, X.Y. Chen, H.J. Dai, Nat. Nanotech. 2, 47 (2007).

[5] R. Weissleder, K. Kelly, E.Y. Sun, T. Shtatland, L. Josephson, Nat. Biotechnol. 23, 1418 (2005).

[6] T. Torchynska, Yu. Vorobiev. Semiconductor II-VI Quantum Dots with Interface States and Their Biomedical Applications, Advanced Biomedical Engineering, Gaetano D. Gargiulo and Alistair McEwan (Eds.), InTech Publisher, Croatia, pp. 143-182, 2011.

[7] L.J. Yang, Y.B. Li, Analyst 131, 394 (2006).

[8] I. Brigger, C. Dubernet, P. Couvreur, Adv. Drug Deliv. Rev. 54, 631 (2002).

[9] Y. Ebenstein, T. Mokari, U. Banin, J. Phys. Chem. B 108, 93 (2004).

[10] F. Wang, W.B. Tan, Y. Zhang, X. Fan, M. Wang, Nanotechnology 17, R1-R13 (2006).

[11] M. Kuno, D.P. Fromm, H.F. Hamann, A. Gallagher, D.J. Nesbitt, J. Chem. Phys.115, 1028 (2001).

[12] A.R. Clapp, I.L. Medintz, J.M., Mauro, Br.R. Fisher, M.G. Bawendi, H. Mattoussi, J. Am. Chem. Soc. 126, 301 (2004).

[13] N. Tessler, V. Medvedev, M. Kazes, S.H. Kan, U. Banin, Science 295, 1506 (2002).

[14] Th.E. Rasmussen, L. Jauffred, J. Brewer, S. Vogel, E.R. Torbensen, B.Ch. Lagerholm, L. Oddershede, E.C. Arnspang, J. Mod. Phys. 4, 27 (2013).

[15] K. Koenig, J. Microsc. 200, 83 (2000).

[16] H.M.E. Azzazy, M.M.H. Mansour, S.C. Kazmierczak, Clin. Biochem. 40, 917 (2007).

[17] C.H. Lin, L.W Chang, H. Chang, M.H. Yang, Ch.Sh. Yang, W.H. Lai, W.H. Chang, P. Lin, Nanotechnology 20, 215101 (2009).

[18] B.A. Fowler, Toxicol. Appl. Pharmacol. 238, 294 (2009).

[19] W.J. Parak, D. Gerion, D. Zanchet, A.S. Woerz, T. Pellegrino, Ch. Micheel, Sh. C. Williams, M. Seitz, R.E. Bruehl, Z. Bryant, C. Bustamante, C.R. Bertozzi, A. P. Alivisatos, Chem. Mater. 14, 2113 (2002).

[20] A. Wolcott, D. Gerion, M. Visconte, J. Sun, Ad. Schwartzberg, Sh. Chen, J. Z. Zhang, J. Phys. Chem. B 110, 5779 (2006).

[21] D. Gerion, F. Pinaud, Sh.C. Williams, W.J. Parak, D. Zanchet, Sh. Weiss, A. P. Alivisatos, J. Phys. Chem. B 105, 8861 (2001).

[22] T.V. Torchynska, Nanotechnology 20, 095401 (2009).

[23] X. Ji, J. Zheng, J. Xu, V.K. Rastogi, T.Ch. Cheng, J.J. DeFrank, R.M. Leblanc, J. Phys. Chem. B 109 (2005) 3793.

[24] L.G. Vega Macotela, J. Douda, T.V. Torchynska, R. Peña Sierra, L. Shcherbyna, Phys. Status Solidi (c) 7, 724 (2010).

[25] W. Guo, J. Jack Li, J.A. Wang, X. Peng, Chem. Mater. 15, 3125 (2003).

[26] T.V. Torchynska, J. Douda, P.A. Calva, S.S. Ostapenko, R. Peña Sierra, J. Vac. Sci. Technol. 27(2), 836 (2009).

[27] T.Y. Ohulchanskyy, A.M. Pliss, P.N. Prasad, Biophotonics: harnessing light for biology and medicine, B. Di Bartolo and J. Collins (Eds.), Biophotonics: Spectroscopy, Imaging, Sensing, and Manipulation, Springer Science+Business Media B.V., 2011, p. 3.

[28] T.V. Torchynska, J. Douda, S.S. Ostapenko, S. Jimenez-Sandoval, C. Phelan, A. Zajac, T. Zhukov, T. Sellers, J. Non-Crystal. Solids, 354, 2885 (2008).

[29] http://www.lifetechnologies.com/ua/en/home/brands/invitrogen.html

[30] [30]http://www.lifetechnologies.com/ua/en/home/life-science/cell-analysis/qdots-microspheres-nanospheres.html?ICID=ta-lm-quantumdots-QuantumDot&Microspheres

[31] A.L. Quintos Vazquez, T.V. Torchynska, J.L. Casas Espinola, J.A. Jaramillo Gómez, J. Douda, J. Luminesc. 143, 38 (2013).

[32] A.Y. Nazzal, X. Wang, L. Qu, W. Yu, Yu. Wang, X. Peng, M. Xiao, J. Phys. Chem. B 108, 5507 (2004).

[33] R.W. Meulenberg, T. Jennings, G.F. Strouse, Phys. Rev. B 70, 235311 (2004).

[34] M. Dybiec, G. Chomokur, S. Ostapenko, A. Wolcott, J.Z. Zhang, A. Zajac, C. Phelan, T. Sellers, G. Gerion, Appl. Phys. Lett. 90, 263112 (2007).

[35] X. Gao, W.C.W. Chan, Sh. Nie, J. Biomed. Opt. 7(4), 532 (2002).

[36] P.A. Temple, C.E. Hathaway, Phys. Rev. B 7, 3685 (1973).

[37] F.A. Johnson, R. Loudon, Proc. R. Soc. A 281, 274 (1964).

[38] N.E. Korsunskaya, I.V. Markevich, T.V. Torchinskaya, M.K. Sheinkman, Phys. Status Solidi (a) 60, 565 (1980).

[39] T.V. Torchynska, A. Diaz Cano, M. Dybic, S. Ostapenko, M. Morales Rodrigez, S. Jimenes Sandoval, Y. Vorobiev, C. Phelan, A. Zajac, T. Zhukov, T. Sellers, Phys. Status Solidi (c) 4, 241 (2007).

[40] T.V. Torchynska, J. Douda, R. Peña Sierra, Phys. Status Solidi (c) 6, S143 (2009).

[41] A. Diaz Cano, S. Jiménez Sandoval, Y. Vorobiev, F. Rodriguez Melgarejo, T. V. Torchynska, Nanotechnology 21, 134016 (2010).

[42] V. Torchynska, J.L. Casas Espinola, A. Díaz Cano, J. Douda, K. Gazarian, Physica E, 51, 60 (2013).

[43] S.A. Empedocles, M.G. Bawendi, Science 278, 2114 (1997).

[44] D.J. Norris, A. Sacra, C.B. Murray, M.G. Bawendy, Phys. Rev. Lett. 72, 2612 (1994).

[45] D.B. Tran Thoai, Y.Z. Hu, S.W. Koch, Phys. Rev. B 41, 6079 (1990).

[46] T.V. Torchynska, Y.V. Vorobiev, V.P. Makhniy, P.P. Horley, Physica B, 453 68 (2014).

[47] P.P. Horley, P. Ribeiro, V.R. Vieira, J. González-Hernández, Yu.V. Vorobiev, L.G. Trápaga-Martínez, Physica E 44, 1602 (2012).

[48] D.J. Norris, M.G. Bawendi, Phys. Rev. B 53, 16338 (1996).

[49] C. Kittel, Introduction to Solid State Physics, 6th ed., John Wiley, NewYork,1986. 1986.

[50] Physics of II-VI compounds, A.N. Georgobiany and M.K. Sheinkman (Eds.), Publisher "Nauka," Moscow, Russia, 1986, 300 p.

[51] Physics and chemistry of II-VI compounds, M. Aven, J.S. Prener (Eds.), North-Holland, Amsterdam, 1967, p. 625.

[52] T.V. Torchynska, J. Luminesc. 137, 157 (2013).

[53] X. Xia, Z. Liu, G. Du, Y. Li, M. Ma, J. Phys. Chem. C 114, 13414 (2010).

[54] T.V. Torchynska, J.L. Casas Espinola, J.A. Jaramillo Gómez, J. Douda, K. Gazarian Physica E, 51, 55 (2013).

[55] A.G. Milnes, D.L. Feucht, Heterojunctions and Metal-Semiconductor junctions, Academic Press, New York, 1972.

[56] Y. Kayanuma, Phys. Rev. B. 38, 9797 (1988).

[57] N.E. Korsunskaya, I.V. Markevich, T.V. Torchinskaya, M.K. Sheinkman, J. Phys. Chem. Solids 43, 475 (1982).

[58] T.V. Torchynska, Physica E 68, 87 (2015).

IntechOpen